

Research Article

Evaluating therapeutic potential of AYUSH-64 constituents against omicron variant of SARS-CoV-2 using ensemble docking and simulations

Vinod Jani^{a,1}, Shruti Koulgi^{a,1}, Mallikarjunachari V.N. Uppuladinne^{a,1}, Saket Ram Thrigulla^{b,d,**}, Manohar Gundeti^c, Goli Penchala Prasad^b, Sanjaya Kumar^d, Srikanth Narayanam^d, Uddhavesht Sonavane^{a,*}, Rajendra Joshi^a

^a High Performance Computing - Medical and Bioinformatics Applications Group, Centre for Development of Advanced Computing (C-DAC), Panchawati, Pashan, 411 008, Pune, India

^b Central Council for Research in Ayurvedic Sciences (CCRAS)-National Institute of Indian Medical Heritage, 500036, Hyderabad, India

^c Central Council for Research in Ayurvedic Sciences (CCRAS)-Central Ayurveda Research Institute, 400018, Mumbai, India

^d Central Council for Research in Ayurvedic Sciences (CCRAS), 110058, New Delhi, India



ARTICLE INFO

Handling Editor Name: Renzhi Cao

Keywords:

Ayush64

Phytochemicals

Ayurveda

MD simulations

Ensemble docking

ABSTRACT

The COVID-19 pandemic in the later phase showed the presence of the B.1.1.529 variant of the SARS-CoV-2 designated as Omicron. AYUSH-64 a poly herbal drug developed by Central Council for Research in Ayurvedic Sciences (CCRAS) has been recommended by Ministry of Ayush in asymptomatic, mild to moderate COVID-19 patients. One of the earlier, *in-silico* study has shown the binding of the constituents of AYUSH-64 to the main protease (M^{Pro}) of the SARS-CoV-2. This study enlisted four phytochemicals of AYUSH-64, which were found to have significant binding with the M^{Pro}. In continuation to the same, the current study proposes to understand the binding of these four phytochemicals to main protease (M^{Pro}) and receptor binding domain (RBD) of spike protein of the Omicron variant. An enhanced molecular docking methodology, namely, ensemble docking has been used to find the most efficiently binding phytochemical. Using molecular dynamics (MD) simulations and clustering approach it was observed that the M^{Pro} and RBD Spike of Omicron variant of SARS-CoV-2 in complex with human ACE2 tends to attain 4 and 8 conformational respectively. Based on the docking studies, the best binding phytochemical of the AYUSH-64, akummicine N-oxide was selected for MD simulations. MD simulations of akummicine N-oxide bound to omicron variant of M^{Pro} and RBD Spike-ACE complex was performed. The conformational, interaction and binding energy analysis suggested that the akummicine N-oxide binds well with M^{Pro} and RBD Spike-ACE2 complex. The interaction between RBD Spike and ACE2 was observed to weaken in the presence of akummicine N-oxide. Hence, it can be inferred that, these phytochemicals from AYUSH-64 formulation may have the potential to act against the Omicron variant of SARS-CoV-2.

1. Introduction

The most lethal wave of the COVID-19 pandemic was due to the B.1.1.529 variant of SARS-CoV-2, designated as Omicron variant. Several therapeutic and preventive approaches have gained impetus since the onset of this infectious disease. Small molecules, monoclonal antibodies, nanodrugs and ayurvedic medicine have been explored extensively to identify their potential as treatment against COVID-19 (Cha-Silva et al., 2024; Allerton et al., 2024; Yamamoto and Inoue,

2024; Tang et al., 2020; Medhi et al., 2020; H Ali et al., 2022).

In India, right from the onset of the COVID-19, the Ministry of Ayush had recommended the use of AYUSH-64 to fight against the symptoms of this disease. AYUSH-64 a polyherbal formulation developed by Central Council of Research in Ayurvedic Sciences (CCRAS) for the malaria, fevers and inflammatory arthritis conditions. AYUSH-64 showed uncomplicated recovery and good safety when administered along with standard symptomatic treatment in Flu-like-illness (Gundeti et al., 2022). Further it has been repurposed for the management of COVID-19

* Corresponding author.

** Corresponding author. Central Council for Research in Ayurvedic Sciences (CCRAS)-National Institute of Indian Medical Heritage, 500036, Hyderabad, India.

E-mail addresses: dr.sakethram@gmail.com (S.R. Thrigulla), uddhaveshts@cdac.in (U. Sonavane).

¹ authors with equal contribution.

<https://doi.org/10.1016/j.crstbi.2024.100151>

Received 28 March 2024; Received in revised form 7 May 2024; Accepted 27 May 2024

Available online 31 May 2024

2665-928X/© 2024 Published by Elsevier B.V. This is an open access article under the CC BY-NC-ND license (<http://creativecommons.org/licenses/by-nc-nd/4.0/>).

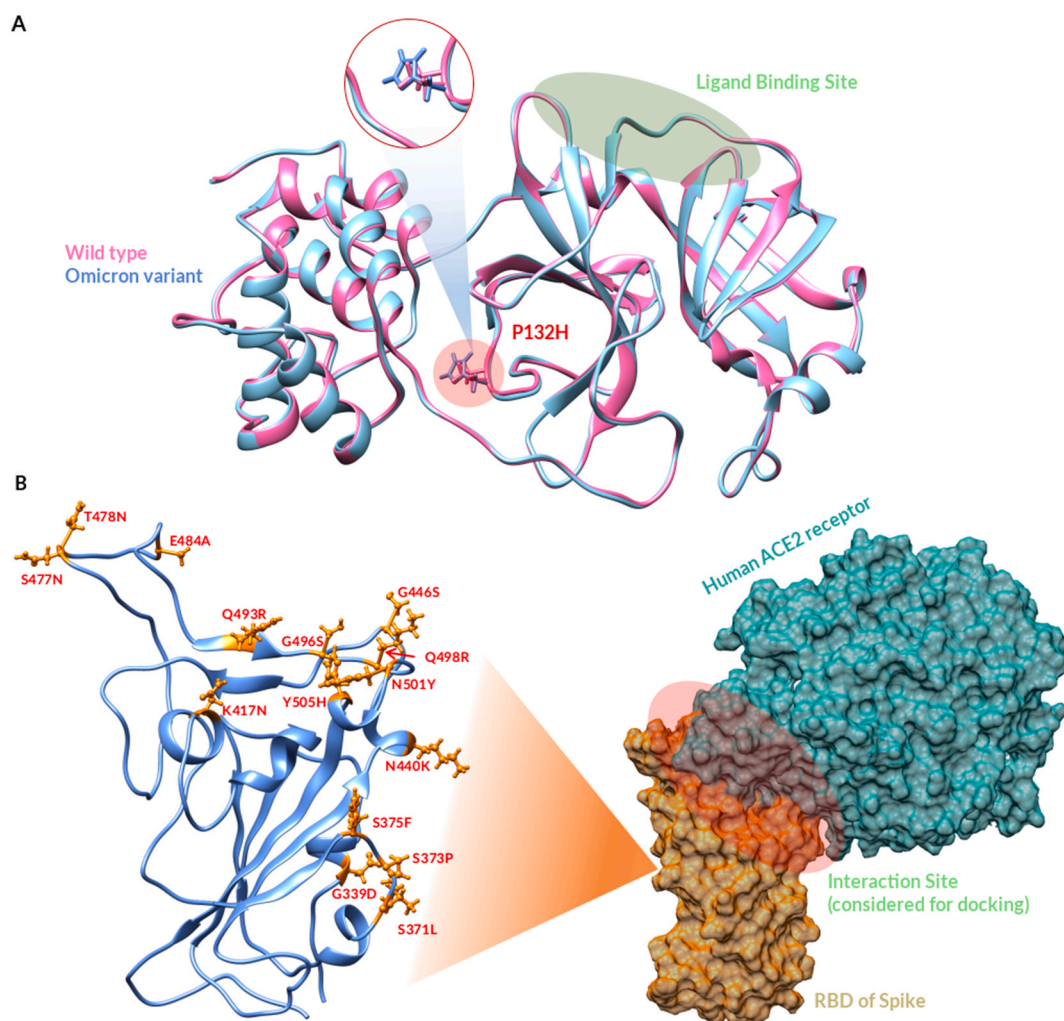


Fig. 1. (A) Main protease (M^{PRO}) and (B) receptor binding domain (RBD) of spike protein from the Omicron variant of SARS-CoV-2.

and has shown to be a significantly effective and safe adjunct in the treatment of mild and moderate COVID-19 in a prospective and randomized controlled drug trial. AYUSH 64 hastened clinical recovery, reduced hospitalization period, and showed early persistent health benefits with minimal/absent drug-related side effects (Chopra et al., 2023). Incidentally in the large community study, Ayush 64 found to provide good therapeutic care to patients with asymptomatic, mild, and moderate COVID-19 in home isolation too (Srikanth et al., 2022). Meta-analysis suggested that add-on AYUSH-64 likely provides therapeutic benefits by reducing time to symptom resolution (mean difference [MD] 2.35 days lower [95% confidence interval, CI; 4.05 lower to 0.65 lower]) and hastening clinical improvement (365 more per 1000 [95% CI; 4 more to 1000 more]) in mild-to-moderate COVID-19 patients (Thakar et al., 2023). One of the earlier *in-silico* studies by a group of Ayurveda professionals and computational biologists had shown the binding of the constituents of AYUSH-64 to the SARS-CoV-2 drug targets (Ram et al., 2022). Based on the four efficient phytochemicals identified back then, the current study proposes to understand their binding to the main protease (M^{PRO}) and receptor binding domain (RBD) of spike protein have from the Omicron variant. An enhanced molecular docking methodology, namely, ensemble docking has been used in this particular study. Ensemble docking method involves docking of desired small molecules to different structural conformations (ensemble representatives) of the target protein, rather than only a single structural conformation obtained from PDB. Molecular dynamics (MD) simulations accompanied by statistical methods such as clustering is used to extract

different structural conformations of the target proteins (drug targets). Similar ensemble docking approach was used for the wild type SARS-CoV-2 in order to perform drug repurposing studies (Koulgi et al., 2021; Jani et al., 2021). Fig. 1 shows the two drug targets, namely M^{PRO} (Fig. 1A) and RBD Spike-ACE2 (Fig. 1B) and their mutations as observed in the Omicron variant of SARS-CoV-2. The ligand binding regions in these targets have also been marked. The grid/energy scores were able to clearly show that the binding of these phytochemicals is either same or improved in case of the Omicron variant as compared to the wild type protein. The details of the methodology followed as well as the results obtained have been discussed further.

2. Methodology

2.1. Model generation

The SWISSMODEL server was used for building the structure of the M^{PRO} omicron variant, having a single mutation at 132nd position. The proline at this position is mutated to histidine (Fig. 1A). The wild type M^{PRO} structure with PDB ID 6LU7 was used as a template to build the mutant structure (Jin et al., 2020). Similarly, the receptor binding domain (RBD) of Spike protein of the Omicron variant of SARS-CoV-2 in complex with ACE2 was built. The Omicron variant has 15 mutations in the RBD of the spike protein, the positions and the residues have been shown in Fig. 1 B. The template used to build the mutant RBD was the PDB structure of wild type spike protein in complex with human ACE2

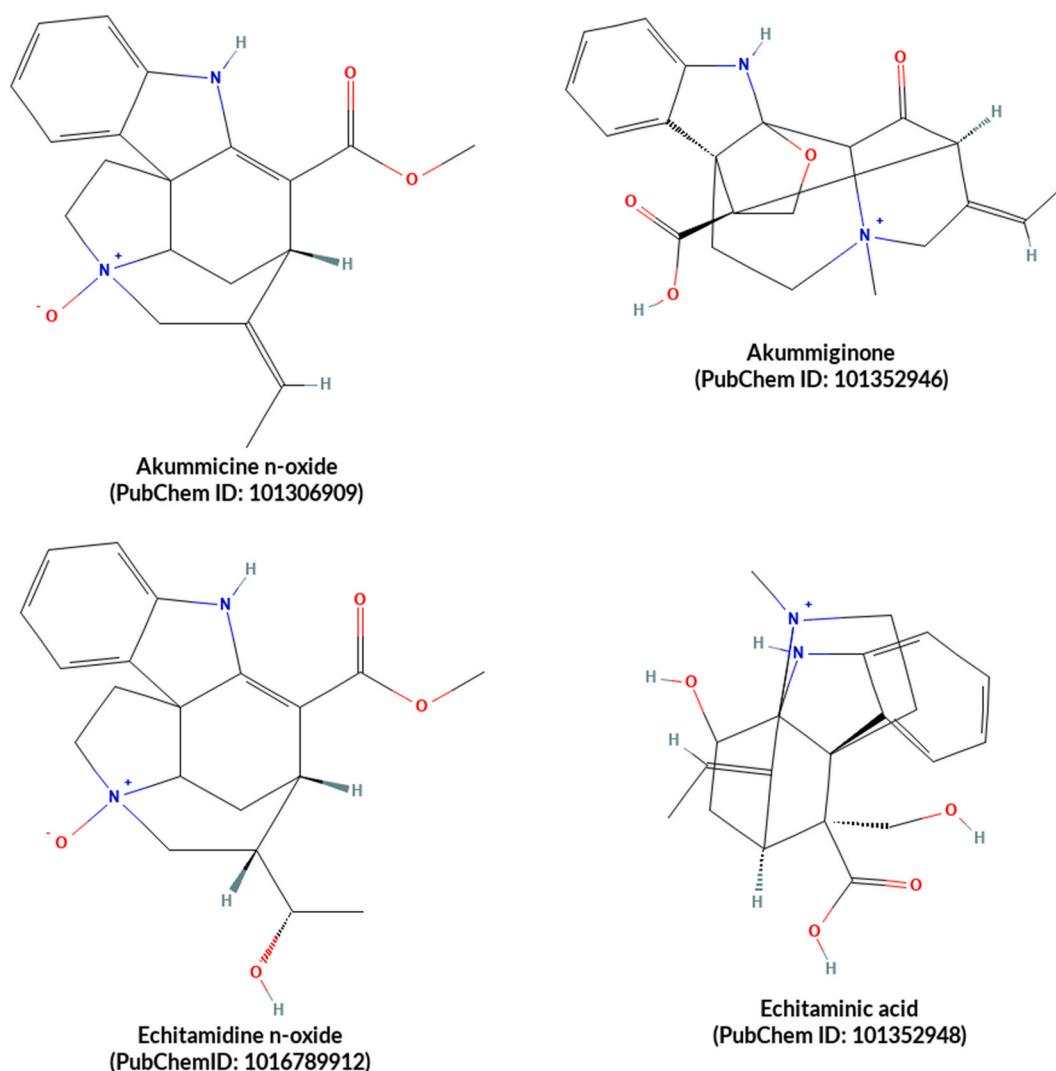


Fig. 2. Phytochemicals with their PubChem CIDs from the AYUSH-64 formulation that have been considered for the molecular docking study.

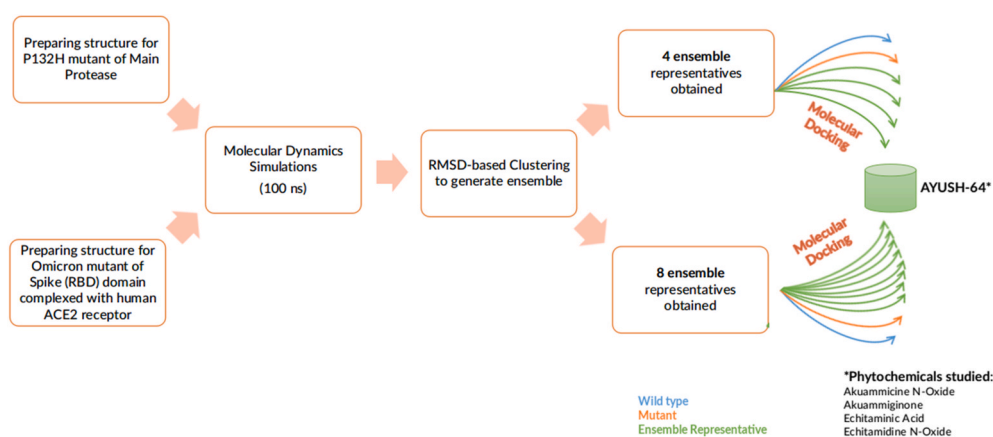


Fig. 3. Detailed outline of the methodology followed for ensemble docking of M^{PRO} and RBD Spike-ACE2 systems.

receptor with PDB ID 6LZG (Wang et al., 2020). The modelled M^{PRO} and RBD spike-ACE2 complex were considered for docking and simulation studies.

2.2. Ensemble docking

The phytochemicals belonging to the Ayush-64 formulation were screened against the mutated M^{PRO} and Spike-ACE2 complex. In one of our earlier studies on these phytochemicals, four of the top ranked compounds were observed to show better binding to the drug targets of

SARS-CoV-2 (Ram et al., 2022; Koulgi et al., 2021). Fig. 2 shows the two dimensional representation and PubChem CIDs for the four phytochemicals that were considered for this study.

The detailed methodology of ensemble docking of these phytochemicals onto the M^{pro} and spike-ACE2 complex of the Omicron variant of SARS-CoV-2 has been shown in Fig. 3.

The molecular dynamics (MD) simulations of M^{pro} and spike-ACE2 complex structures were performed using the 2020.2 version of GRO-MACS simulation package (Spoel et al., 2005). Similar protocol was followed for both the proteins. The parameters were generated using AMBER FF14SB force field (Maier et al., 2015). The TIP3P water model was used for representing the water molecules. The systems were neutralized by adding Na⁺ ions. The systems were minimized for around 20,000 steps of steepest descent followed by the conjugate gradient method. Further, they were equilibrated in two steps, first being NVT equilibration for around 500 ps followed by NPT equilibration of around 1 ns. In the NVT equilibration the system was heated gradually up to 300 K using the Langevin thermostat (Davidchack et al., 2009). The NPT equilibration was carried out with temperature maintained around 300 K and pressure at 1 atm. This was followed by two sets of production runs of 50 ns for each system, making a cumulative time of 100 ns for each system. RMSD-based clustering was performed for both the systems. The dbscan method from the cpptraj module of AmberTools17 was used for the RMSD-based clustering with a RMSD cut-off of 1.5 Å (Ester et al., 1996). A total of 4 and 8 ensemble representative (Erep) structures were obtained for M^{pro} and spike-ACE2 complexes respectively. Along with these Erep structures, the wild type and the initial modelled structures of the mutated protein were docked with the selected phytochemicals from AYUSH-64.

The DOCK6 program was used for the docking (Allen et al., 2015).

The receptor file was used to select spheres in the receptor during the process of receptor preparation by the DOCK6 program. Hydrogen atoms were removed and the surface of the receptor binding site was calculated with probe radius of 1.4 Å by using the DMS program in the DOCK6. Receptor spheres were generated using the program *sphgen*. Spheres covering the hotspot were selected within 10 Å from the ligand binding residues of the receptor. The grid box that enclosing the selected spheres was generated with an extra 5 Å added in each dimension. Ligand rigidity was employed during the docking process using the DOCK6 module with output presented as grid scores.

The binding efficiency of the drugs were elucidated based on their grid score. The grid scores calculated by DOCK 6, measures the strength of binding of any small molecule in terms of the non-bonded interactions formed with the active site of the receptor molecule. The grid scores are energy values which are obtained using force field equation given below,

$$E = \sum_{i=1}^{lig} \sum_{j=1}^{rec} \left(\frac{A_{ij}}{r_{ij}^a} - \frac{B_{ij}}{r_{ij}^b} + 332 \frac{q_i q_j}{D r_{ij}} \right)$$

Where, E is the grid score and $\frac{A_{ij}}{r_{ij}^a} - \frac{B_{ij}}{r_{ij}^b}$ is the van der Waals contribution and $332 \frac{q_i q_j}{D r_{ij}}$ is the electrostatic contribution. Each of these terms are in double summation over ligand atoms i and receptor atoms j. A more negative value of E, indicates better stability of docking obtained by that particular molecule. The details of choosing top scored ligands from ensemble docking has been discussed in detail in the 'Results & Discussion' section.

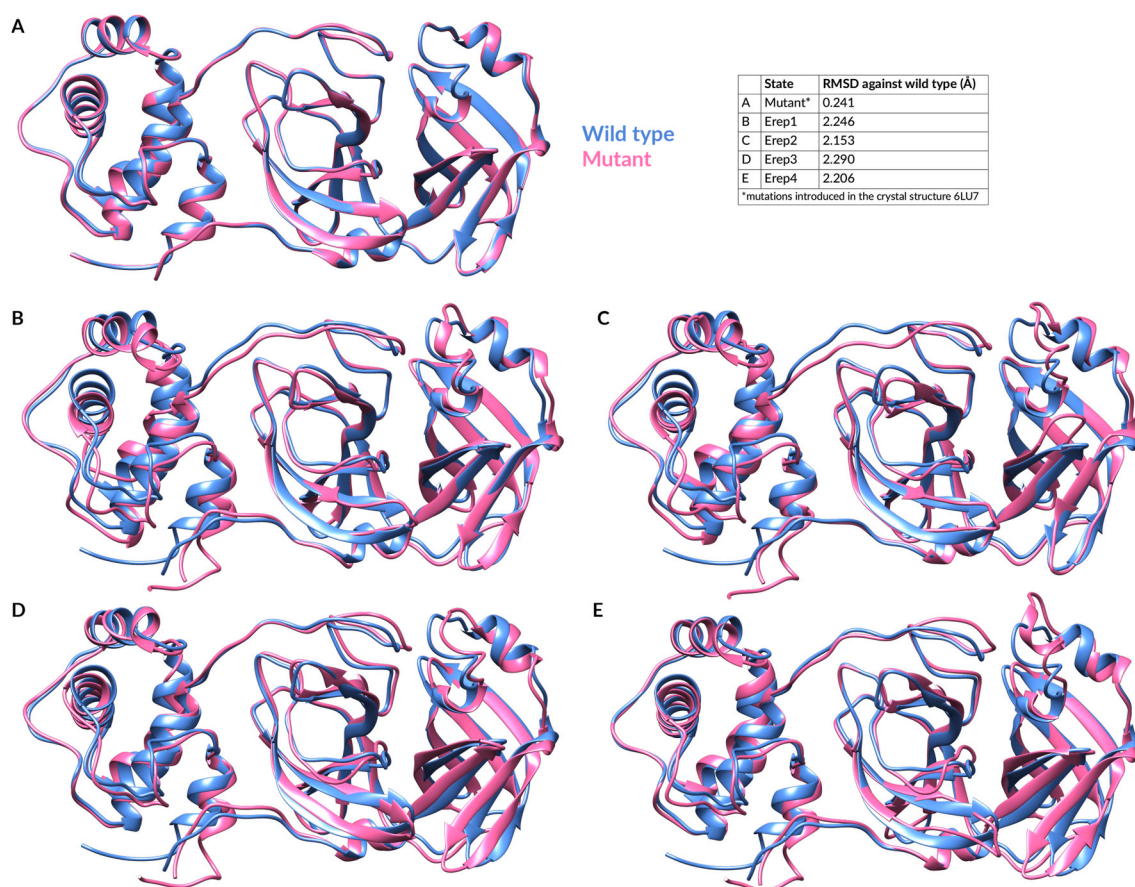


Fig. 4. Comparison between the (A) mutant and (B-E) different Erep structures of the Omicron variant of M^{pro} and wild type (PDB ID: 6LU7). (Inset table) The all atom RMSD between the representatives and the wild type M^{pro}.

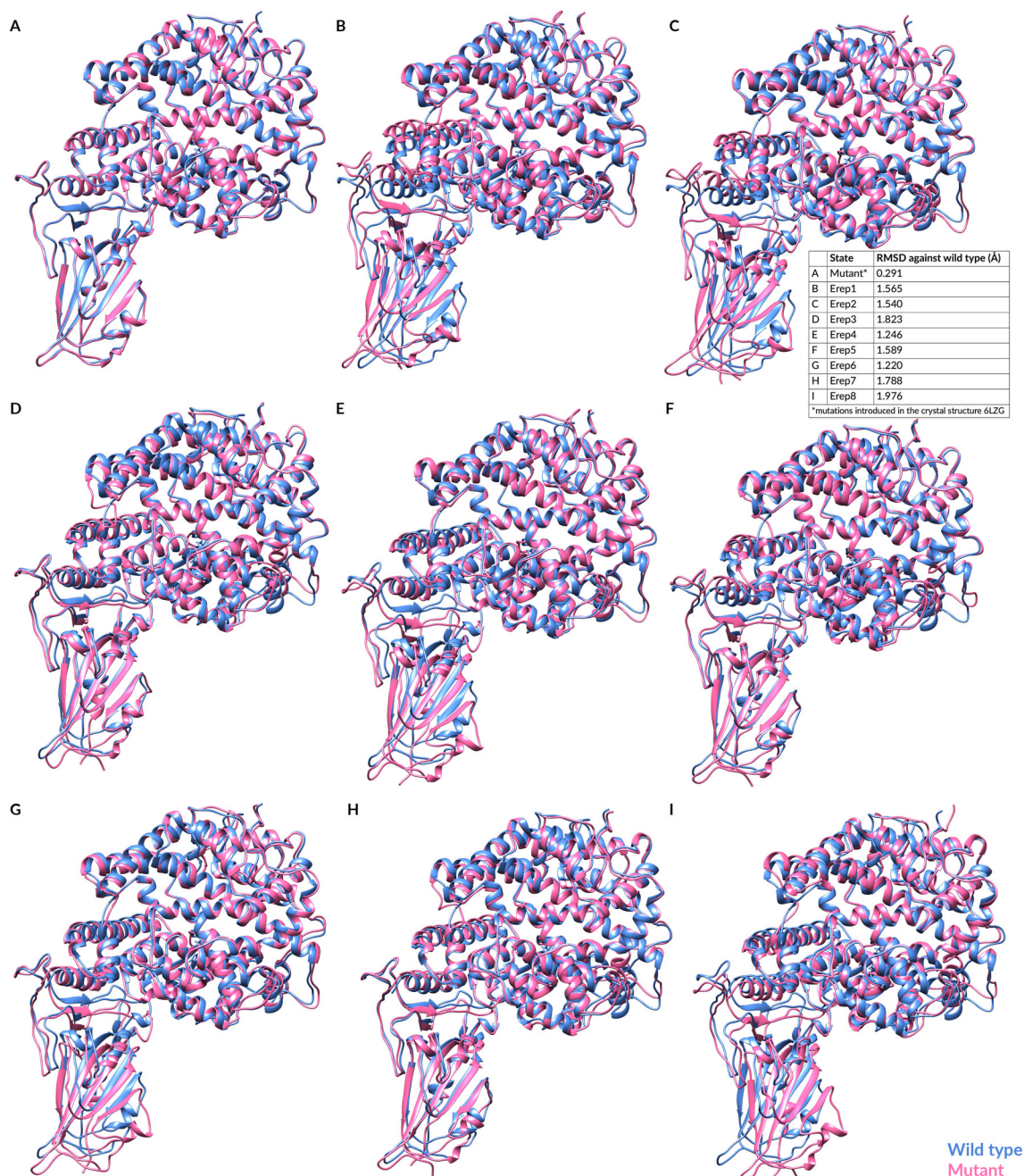


Fig. 5. Comparison between the (A) mutant and (B–I) different Ereps of the Omicron variant of RBD Spike-ACE2 complex and wild type (PDB ID: 6LZG). (Inset table) The all atom RMSD between the representatives and the wild type RBD Spike-ACE2 complex.

2.3. Molecular dynamics

The molecular simulations were performed for the best docked ligand-protein complex for both M^{PRO} and RBD Spike-ACE2 complex. As a control, the simulations were also carried out for the apo systems of the M^{PRO} and RBD Spike-ACE2 protein. All the molecular simulations were carried out using the AMBER20 simulation package. The proteins were represented using AMBER14SB force field parameters (Maier et al., 2015). The parameters for the akuammicine N-oxide were generated using the antechamber module of AMBERTOOLS20 and the force field used was the general atom force field. The docked complex was neutralized using Na^+ ions followed by addition of solvent molecules. The octahedral geometry for the TIP3P water model was used in order to solvate the ligand-bound and apo protein systems. The molecular

dynamics simulations were performed using the classical steps of minimization, temperature ramping, equilibration and production run. The minimization was performed using steepest descent followed by a conjugate gradient method for a cumulative of 10,000 steps. Initially, the solvent was minimized followed by the solute. The entire simulation system was gradually heated up to 300 K using the Berendsen thermostat and Langevin dynamics. The hydrogen atoms were constrained using the SHAKE algorithm. After achieving the desired temperature, an equilibration was performed at a constant temperature of 300 K and a constant pressure of 1 atm for 2 ns. This was followed by the production run of 100 ns for each of the systems.

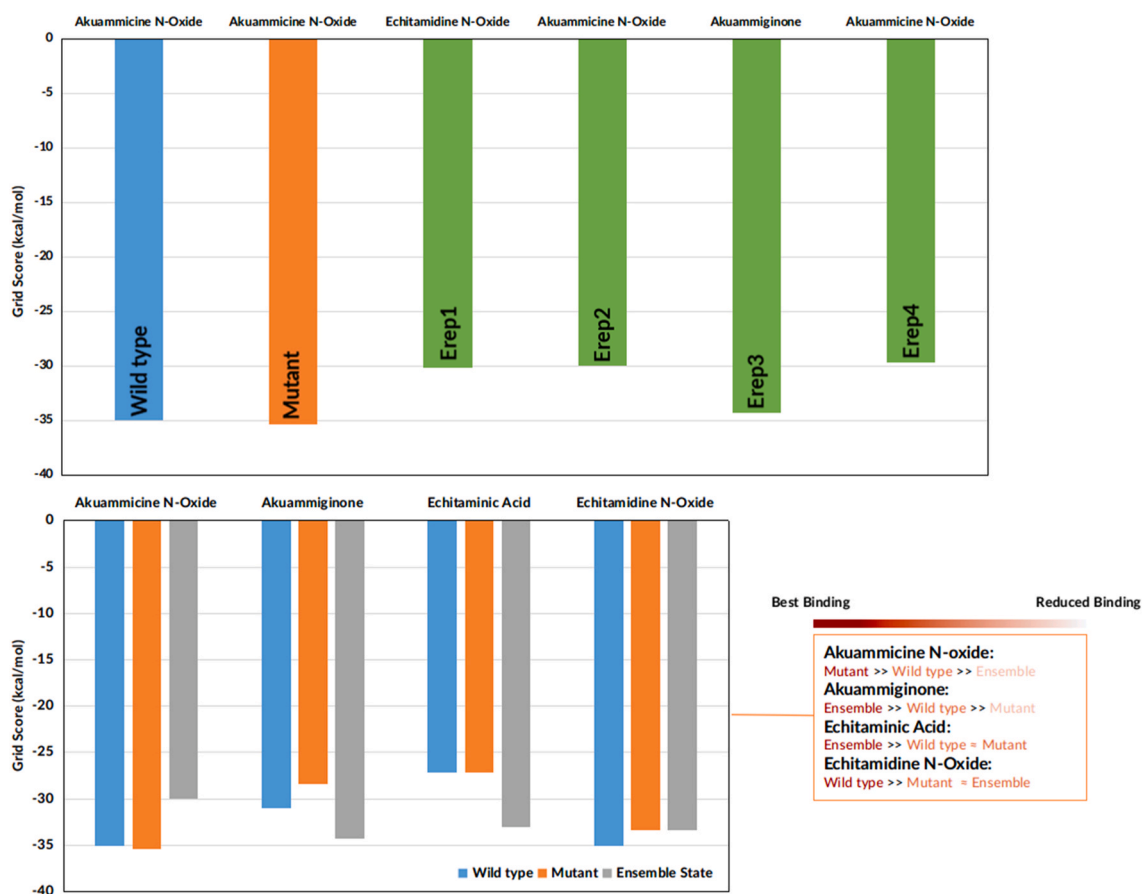


Fig. 6. (A) Grid scores obtained through docking for the best phytochemicals in each ensemble representative and (B) binding of phytochemicals in wild type, mutant and ensemble states for M^{PRO}.

2.4. Analysis

The ADME properties of the phytochemicals were calculated using swissADME server (Daina et al., 2017). The principal component analysis (PCA), interaction analysis and structural analysis for molecular simulation trajectories were performed using the cpptraj module of AMBERTOOLS20 (AMBER, 2020, 2020). The fluctuations were visualized using the Normal Mode Wizard (NMWiz) plugin of Visual Molecular Dynamics (VMD) (Humphrey et al., 1996). The GetContacts. module of FlarePlot was used for calculating and visualizing the hydrogen bonding and salt bridge interactions between the ligand and protein molecules (GetContacts.). The MMPBSA. py module of AMBERTOOLS20 was used for calculating the free energy of binding between the ligand molecules and the protein and also between protein-protein complexes in case of Spike-ACE2 system (Miller et al., 2012). The equation given below was used for calculating the free energy of binding ($\Delta\Delta G_{\text{bind}}$) between the M^{PRO} and RBD Spike-ACE2 complex and the bound phytochemical,

$$\Delta\Delta G_{\text{bind}} = \Delta G_{\text{complex}} - \Delta G_{\text{receptor}} + \Delta G_{\text{ligand}}$$

$$\Delta G_{\text{complex/receptor/ligand}} = \Delta H_{\text{complex/receptor/ligand}} - T\Delta S_{\text{complex/receptor/ligand}}$$

Where, $\Delta G_{\text{complex}}$, $\Delta G_{\text{receptor}}$, and ΔG_{ligand} stand for the free energy of the M^{PRO} and RBD Spike-ACE2 complex bound to Akuammicine N-oxide, only the protein component and Akuammicine N-oxide, respectively. The enthalpy component, $\Delta H_{\text{complex/receptor/ligand}}$, of the free energy was considered for the calculations.

3. Results and discussion

3.1. Ensemble generation

The data obtained after MD simulations of the M^{PRO} and RBD Spike-ACE2 complex for the Omicron variant of SARS-CoV-2 was subjected to RMSD-based clustering to generate ensemble representatives for both the protein systems (Fig. 3). The structural variation in these ensemble representatives (Erep) for both these protein systems has been discussed further.

The RMSD-based clustering for the Omicron variant of M^{PRO} generated four clusters of ensembles. The representative of each of these four ensembles was considered along with the wild type (PDB ID: 6LU7) and the start structure of the simulations of the mutated M^{PRO} (referred henceforth as Mutant). Fig. 4 pictorially depicts these structures and their comparison with the wild type M^{PRO}. Fig. 4 A shows the start mutant structure superimposed on to the wild type M^{PRO}, which has an RMSD of 0.241 Å. Fig. 4 B-E shows the Erep structures superimposed on to the wild type M^{PRO}, with RMSD ranging between 2.1 Å to 2.3 Å. Hence, a total of 6 structures, namely, wild type, mutant, Erep1, Erep2, Erep3 and Erep4 were considered for docking.

The RMSD-based clustering of Omicron variant of RBD Spike bound to ACE2 resulted in eight ensembles. The representative structure of each of these eight ensembles was considered along with the wild type (PDB ID: 6LZG) and the initial modelled structure of the mutated RBD spike in complex with ACE2 (referred henceforth as Mutant). Fig. 5 pictorially depicts these structures and their comparison with the wild type RBD of spike. Fig. 5 A shows the mutant structure superimposed on to the wild type RBD Spike in complex with ACE2, which had an RMSD of 0.291 Å. Fig. 5 B-I shows the Erep structures superimposed on to the

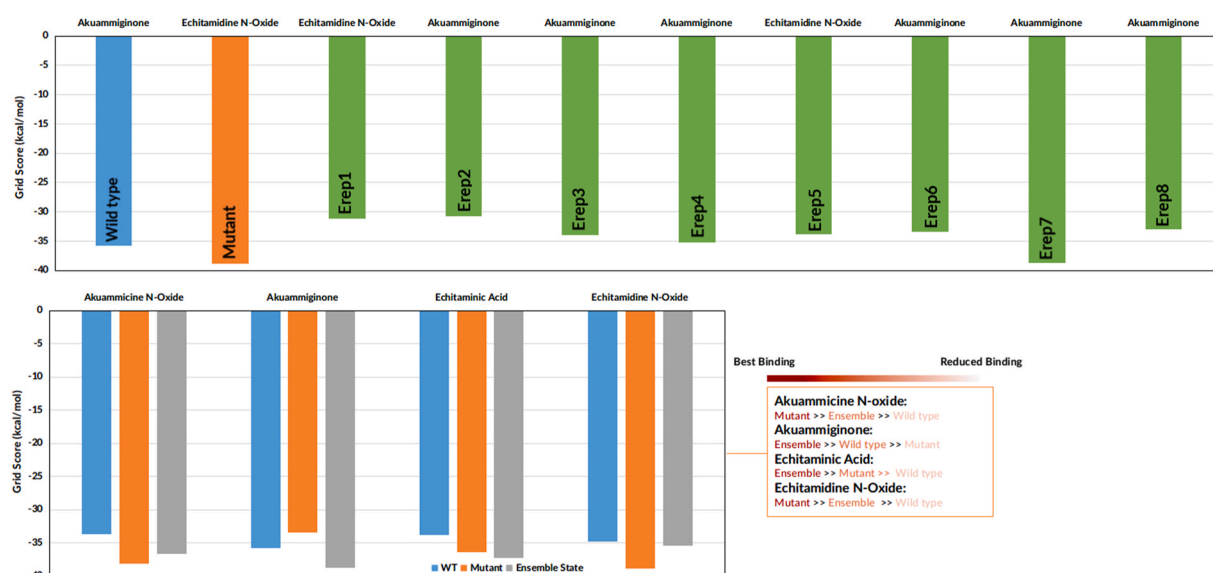


Fig. 7. (A) Grid scores obtained through docking for the best phytochemicals in each ensemble representative and (B) binding of phytochemicals in wild type, mutant and ensemble states for RBD Spike-ACE2 complex.

wild type RBD spike-ACE2 complex, with RMSD ranging between 1.2 Å to 2 Å. Hence, a total of 10 structures, namely, wild type, mutant, Erep1, Erep2, Erep3, Erep4, Erep5, Erep6, Erep7 and Erep8 were considered for docking.

3.2. Binding of phytochemicals

The binding of phytochemicals was analysed based on the grid score obtained through DOCK6 against both the protein systems for all the four phytochemicals. A more negative value of this score indicates better binding of the phytochemical to that particular protein system.

Fig. 6 A depicts the grid scores for the phytochemicals in the wild type, mutant and the four ensemble states (Erep1, Erep2, Erep3 and Erep4) of M^{pro} . The phytochemical akuammicine N-oxide was observed to show best binding to 6LU7 (wild type), mutant, Erep2 and Erep4. On observing the binding energy of the phytochemicals it could be clearly seen that most of them showed improved binding to the mutant, or the mutant ensemble representative of M^{pro} as compared to the wild type protein (Fig. 6 B). In one of the earlier work by Thrigulla Saketh Ram and co-workers, the phytochemical akuammicine N-oxide was observed to show best binding to wild type M^{pro} ¹⁰. In the current study, the binding of this phytochemical with the mutant was also observed to be better than that of the wild type. A energy difference of 2–5 kcal/mol was observed between the wild type and mutant M^{pro} with the latter one showing improved binding in the majority of the phytochemicals.

Fig. 7 A depicts the grid scores for the phytochemicals in different ensemble states of RBD Spike-ACE2 complex. The phytochemical akuammiginone was observed to show best binding to 6LZG, Erep2, Erep3, Erep4, Erep6, Erep7 and Erep8. On observing the binding energy of the phytochemicals it could be clearly seen that most of them showed improved binding to the mutant, or the mutant ensemble representative of RBD of spike in complex with human ACE2 receptor as compared to the wild type (Fig. 7 B). Akuammiginone was observed to have best binding to the mutant ensemble representative, Erep7. All the four phytochemicals were observed to bind with better energy values to the mutant conformations as compared to the wild type. The energy difference between either of the mutant conformations and the wild type was observed to be more than 5 kcal/mol.

The phytochemical akuammicine N-oxide was observed to bind better to the mutant than the wild type for both the proteins M^{pro} and RBD Spike-ACE. Additionally, as mentioned in the earlier docking

studies on the wild type M^{pro} with phytochemicals of AYUSH-64, akuammicine N-oxide was observed to show better binding. Therefore, akuammicine N-oxide was studied further in complex with the mutant M^{pro} and RBD Spike-ACE2 using MD simulations. Classical MD simulations for 100 ns each was performed for this phytochemical-bound complexes of these two protein systems.

3.3. Conformational dynamics of m^{pro}

The conformational variation in the mutant M^{pro} protein in apo form (M^{pro} -Apo) and in complex akuammicine N-oxide (M^{pro} -Aku) were measured based on different structural parameters and principal component analysis (PCA).

3.3.1. Overall structural variation

The overall structural variation was analysed by calculating the root mean square deviation (RMSD) against the start structure of the simulation as well as by observing the changes in the secondary structural elements in presence and absence of akuammicine N-oxide. It was observed that the binding of the ligand leads to conformational rigidity in the structure (Fig. 8 A). The RMSD variation for M^{pro} -Apo was in the range of 2–3.2 Å with maximum conformers having RMSD around 2.7 Å, while for M^{pro} -Aku it was in the range of 1–3.5 Å with maximum conformers were having RMSD around 2 Å. This shows that binding of akuammicine N-oxide brings more rigidity to the structure. Fig. 8 B–C show the secondary structure growth plot along the time for M^{pro} -Apo and M^{pro} -Aku, respectively. From the figure it can be seen that more variation in secondary structure content was observed in the M^{pro} -Apo as compared to that of ligand bound M^{pro} -Aku complex. Variations in M^{pro} -Apo structure were observed for the residues within the range 41–51 and 231 to 241, where helical structure tends to form bend structure. Also, the C-terminal end residue range 291–297 of the M^{pro} -Apo structure shows α to bend conversion.

3.3.2. Dominant conformational changes

The principal component analysis of M^{pro} in both M^{pro} -Apo and M^{pro} -Aku systems was carried out. Fig. 9 A shows RMSF along PC1, from the figure it can be observed that the average variation in M^{pro} -Apo system was in the range of 3–3.5 Å, while the same in M^{pro} -Aku system was in the range of 1.5–2 Å. The region with residue range 5–120 of M^{pro} -Apo system shows more variation as compared to that of M^{pro} -Aku system.

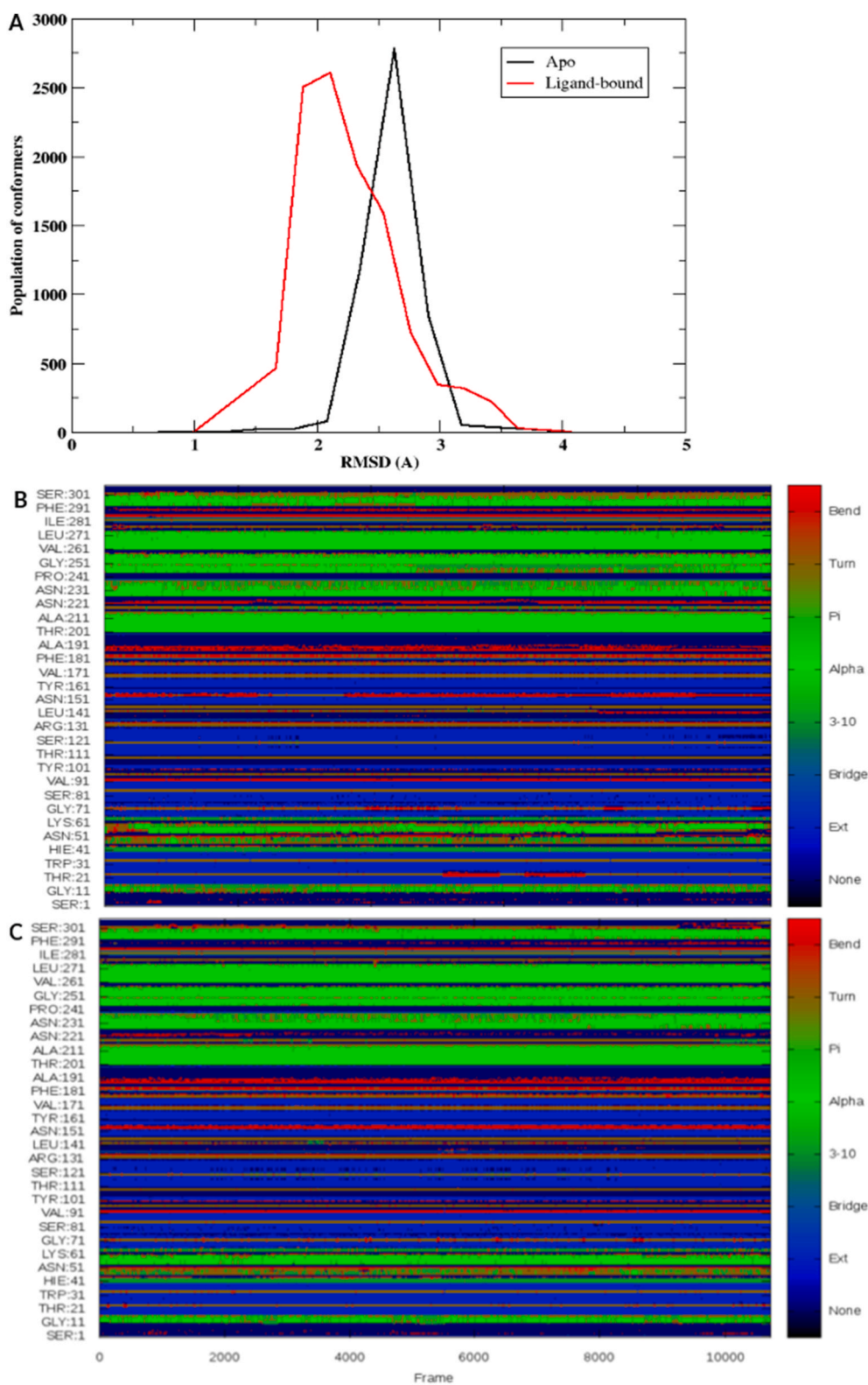


Fig. 8. (A) Distribution of conformers along the RMSD of M^{pro} for M^{pro} -Apo and M^{pro} -Aku complex. (B–C) Secondary structure changes along the simulations of M^{pro} -Apo and M^{pro} -Aku simulations, respectively.

The region with residue range 140–145 showed major fluctuation in M^{pro} -Apo system. Further the variation along the PC2 was observed, the RMSF was plotted for the systems (Fig. 9 B). From the figure, it can be observed that for both the M^{pro} -Apo and M^{pro} -Aku complex, the average variation was in the range of the 2 to 3 Å. However, the region

with residue range 45–60 showed variation of around 7 to 8 Å in the M^{pro} -Apo system.

The variations captured by PC1 were mapped on to the structure of M^{pro} from the M^{pro} -Apo (Fig. 9 C) and M^{pro} -Aku (Fig. 9 D) system. The principal component analysis showed that the major dominant motions

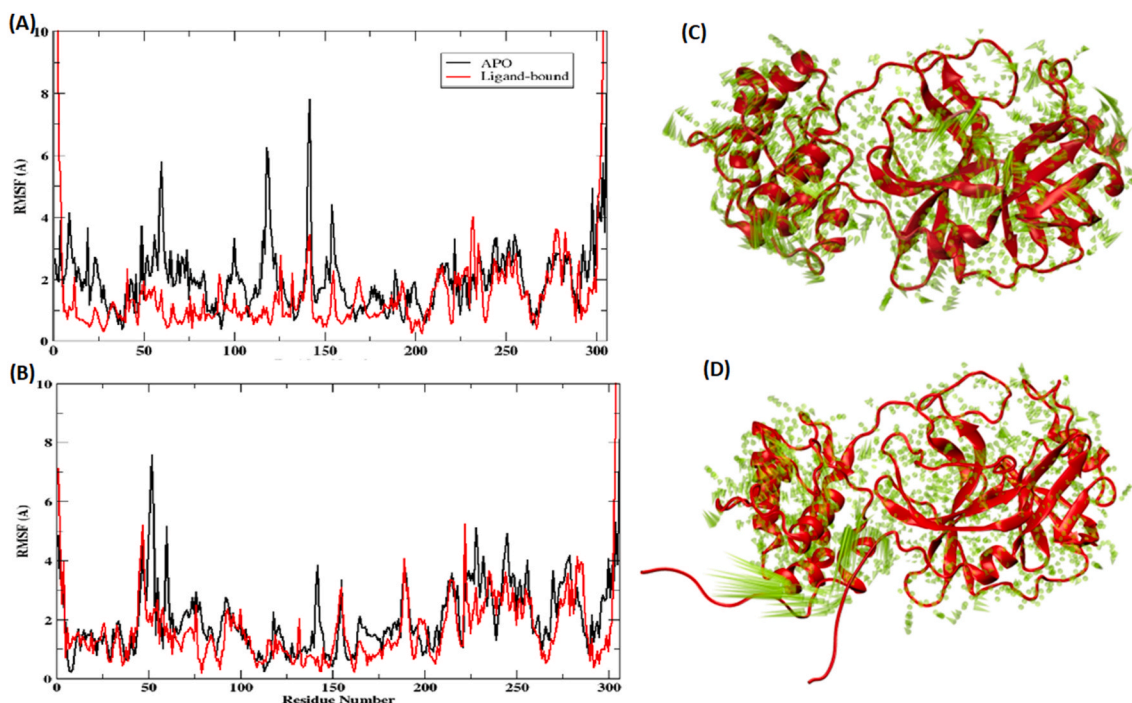


Fig. 9. RMSF for residues of M^{PRO} from M^{PRO} -Apo and M^{PRO} -Aku systems along principal component (A) 1 and (B) 2. Projections of variance for the M^{PRO} in systems (C) M^{PRO} -Apo and (D) M^{PRO} -Aku along PC1.

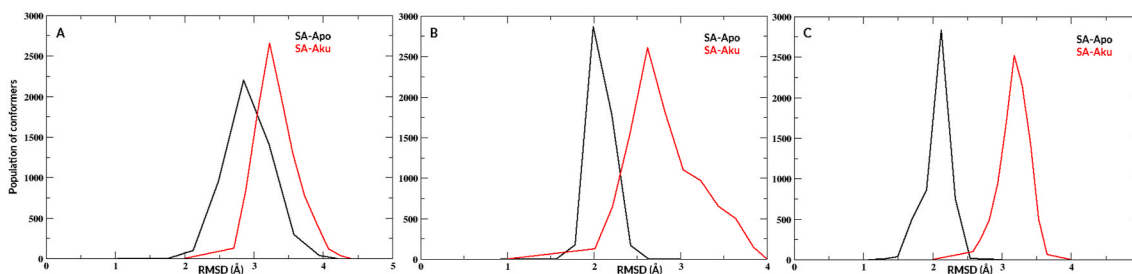


Fig. 10. Distribution of conformers along the RMSD of (A) RBD Spike-ACE2 complex, (B) RBD Spike and (C) ACE2 in SA-Apo and SA-Aku simulation systems.

were mainly observed in the M^{PRO} -Apo system along PC1 lies towards the N-terminal region of protein, especially along residue ranges 10–20, 55–60, 105–120, 140–145 and 150–153.

3.4. Conformational dynamics of RBD Spike-ACE2 complex

The conformational variation in the mutant RBD Spike-ACE2 complex in apo form (SA-Apo) and in complex with akuammicine N-oxide (SA-Aku) were measured based on different structural parameters and principal component analysis (PCA).

3.4.1. Overall structural variation

In order to observe the overall deviation in the RBD Spike-ACE2 structure the RMSD was calculated against the start structure of the simulation. Fig. 10 A, B, and C show the RMSD distribution plot for the entire RBD Spike-ACE2 complex, only RBD Spike and only ACE2 in both the systems, respectively. It can be observed that the binding of the ligand leads to more deviation in the SA-Aku system as compared to the SA-Apo. The RMSD distribution for the entire system, in the case of the SA-Apo system lies in the range of 1.8–4 Å, with majority of conformations having value around 2.8 Å. For the SA-Aku system the RMSD values lie in the range of 2–4.3 Å, with the majority of conformations having value around 3.5 Å. In order to look into the contribution by individual proteins, the RMSD were calculated for the RBD Spike and

ACE2. Fig. 10 B and Fig. 10 C shows RMSD values for the RBD Spike and ACE2 respectively. The RMSD distribution for RBD Spike was narrower in case of SA-Apo as compared SA-Aku (Fig. 10 B). In case of SA-Apo most populated conformer showed RMSD value around 2 Å, whereas for SA-Aku it was around 2.5 Å. In case of ACE2, the RMSD distribution clearly demarcated the conformers belonging to the two systems. The conformers of ACE2 were observed to populate the most around 2 Å and 3.2 Å RMSD values in the SA-Apo and SA-Aku, respectively.

3.4.2. Dominant conformational changes

The principal component analysis of the RBD Spike-ACE2 complex was carried out for both the SA-Apo and SA-Aku systems. Fig. 11 A and B shows the residue-wise RMSF for the RBD Spike protein along PC1 and PC2, respectively. The residues within the range 358–370 and 383–393 appeared to fluctuate the most in both SA-Apo and SA-Aku systems. These fluctuations were captured along both the PCs 1 and 2. However, the residue range 358–370 fluctuated significantly more at PC2 for the SA-Aku system with RMSF ranging between 4 and 11 Å. Similarly, the residue range 383–393 fluctuated considerably more in SA-Aku as compared to SA-Apo with RMSF ranging between 2 and 16 Å. Fig. 11 C and D shows the residue-wise RMSF for the ACE2 protein along PC1 and PC2. In case of ACE2, it was observed that almost all the residues showed similar fluctuation in both systems. A slight difference in the RMSF along PC1 for the residues within 130–140 was observed, where in the values

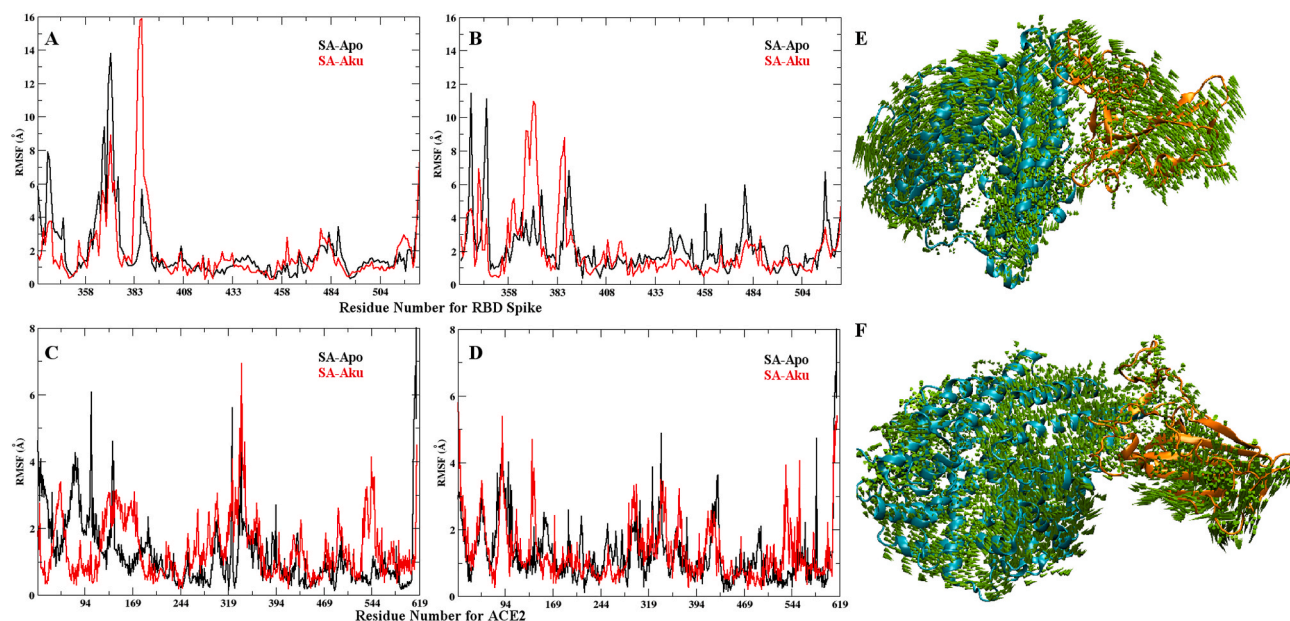


Fig. 11. (A–B) RMSF for the residues of RBD Spike in the SA-Apo (black) and SA-Aku (red) systems along PC1 and PC2, respectively. (C–D) RMSF for the residues of ACE2 in the SA-Apo (black) and SA-Aku (red) systems along PC1 and PC2, respectively. (E–F) Projections of PC1 variation on the RBD Spike-ACE2 complex for the SA-Apo and SA-Aku systems, respectively. (For interpretation of the references to color in this figure legend, the reader is referred to the Web version of this article.)

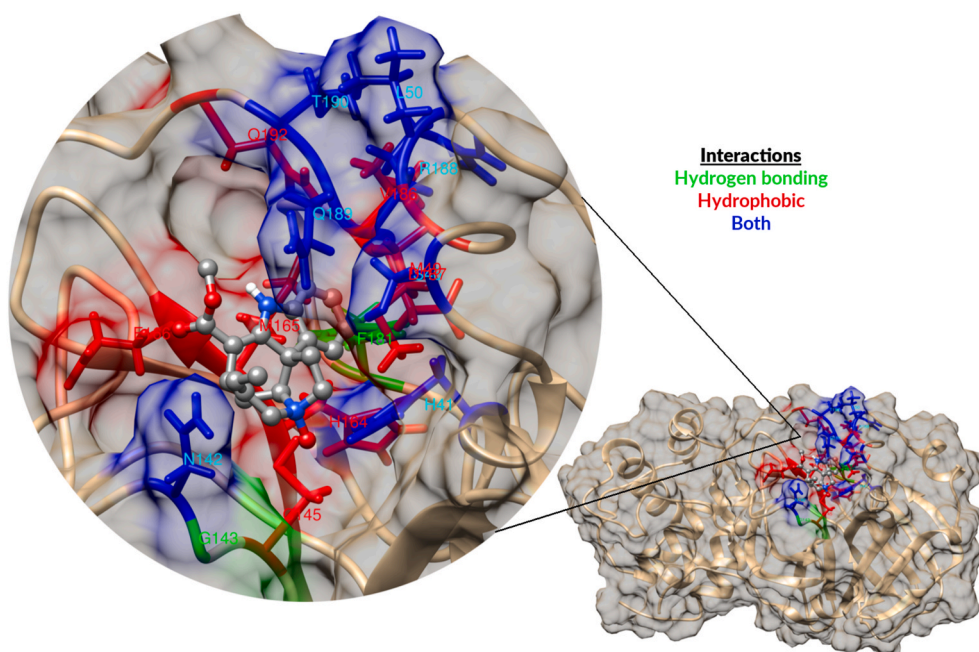


Fig. 12. Residues interacting with akummicine N-oxide in the M^{Pro} -Aku simulation system.

were higher for the SA-Aku system as compared to the SA-Apo. These variations in the residues of RBD Spike and ACE2 were mapped on to the structure in the form of porcupine plots (Fig. 11 E and F). The regions with taller peaks correspond to the region consisting of residues with higher RMSF values.

3.5. Binding of akummicine N-oxide

The binding of akummicine N-oxide to M^{Pro} and SA complex was analysed by identifying the interacting residues from the protein as well as by calculating the MM-GBSA free energy of binding between the protein and the ligand.

3.5.1. Interaction with M^{Pro}

The akummicine-N-oxide mainly forms two types of interactions with M^{Pro} viz. hydrophobic and hydrophilic interactions. The hydrogen bonding and hydrophobic interaction having occupancy more than 20% throughout the simulations have been shown in Fig. 12.

Fig. 12 shows color-labelled residues that formed stable hydrogen bonding (green), hydrophobic (red) and both (blue) interactions with the ligand (shown in grey). The percentage occupancy of these interactions has been given in supplementary figure S1. The binding site of M^{Pro} mainly consists of two subsites S1 and S2 [4]. The subsite S1 consists of F140, G143, C145, H163, E166 and H172. The subsite S2 consists of residues T25, H41, M49, M165 and Q189. Residues G143,

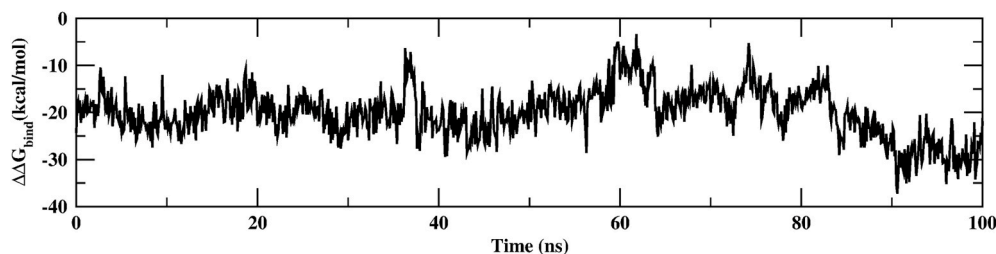


Fig. 13. Free energy of binding ($\Delta\Delta G_{\text{bind}}$) between M^{Pro} and Akummicine N-oxide throughout the simulations.

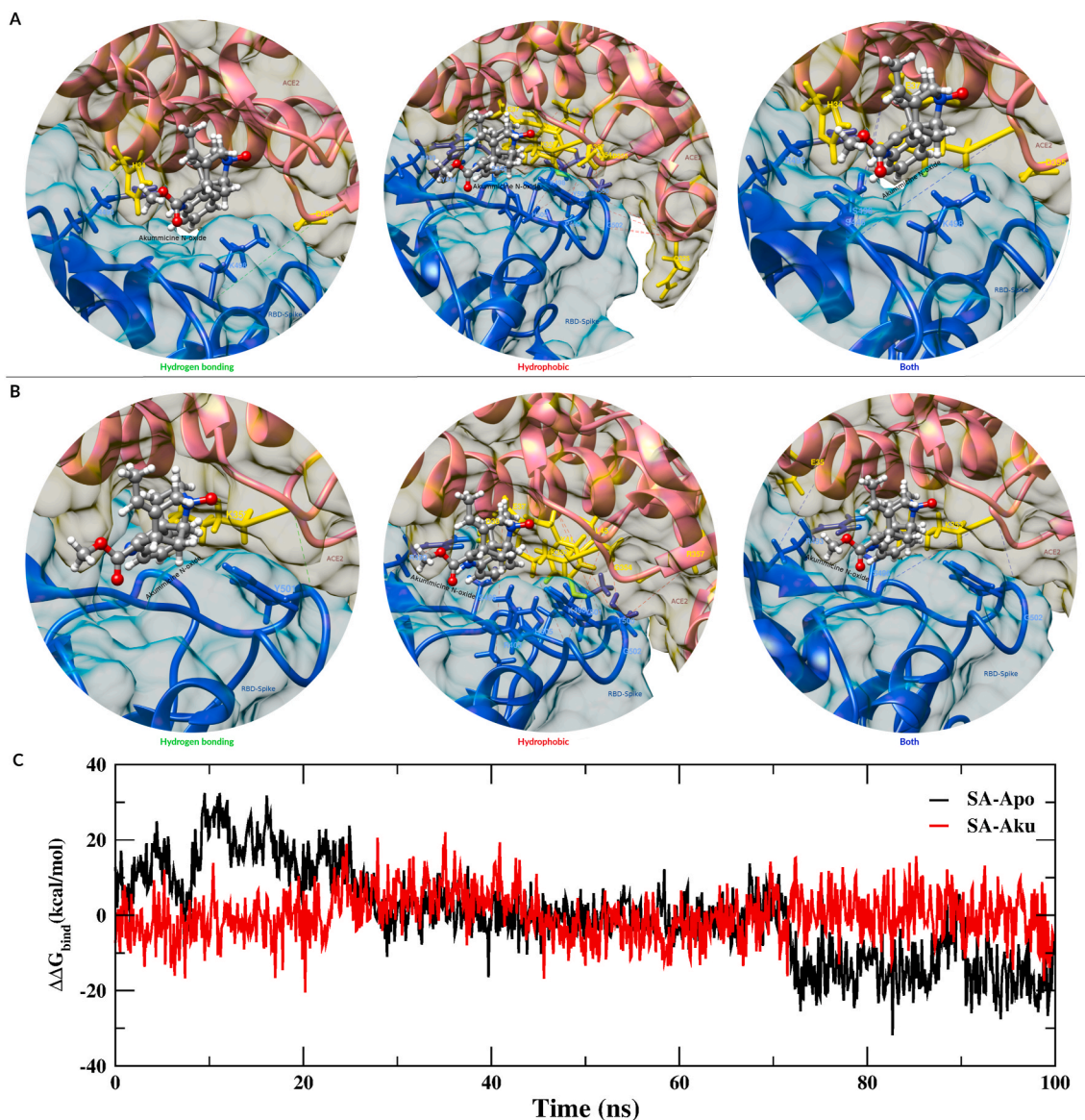


Fig. 14. Interactions between RBD Spike-ACE2 that were (A) lost and (B) gained in the SA-Aku simulation system. (C) $\Delta\Delta G_{\text{bind}}$ between RBD Spike and ACE2 receptors in the SA-Apo (black) and SA-Aku (red) simulation systems. (For interpretation of the references to color in this figure legend, the reader is referred to the Web version of this article.)

C145 and E166 from S1 were observed to form hydrogen bonding and hydrophobic interactions with akummicine N-oxide. G143 was involved in hydrogen bonding whereas the remaining two formed hydrophobic interactions with the ligand. Residues H41, M165 and Q189 from the S2 were observed to be interacting with akummicine N-oxide. H41 and Q189 formed both hydrogen bonding and hydrophobic interactions with the ligand. Whereas, M165 was observed to form only hydrophobic

interactions. Additionally, F181 was observed to form hydrogen bonding interactions with akummicine N-oxide. Few other residues viz. H164, D166, V186, D187 and Q192 which lie in close proximity to the two subsites were observed to form hydrophobic interactions. The residue C145 from S1 is known to form covalent bond with N3 ligand in the crystal structure 6LU7 [4]. This suggests it may be one of the important residues responsible for interacting with ligands. It was also observed to

Table 1

Comparison of hydrogen bonding interactions formed between ACE2 receptor and RBD Spike for wild type RBD Spike, SA-Apo and SA-Aku systems (\checkmark = present x = absent *mutated residue in omicron variant).

Wild type	SA-Apo	SA-Aku
Q24-N487	\checkmark	\checkmark
H34-Y453	x	x
E35-Q493*R	x	\checkmark
E37-Y505	x	x
D38-Y449	\checkmark	x
Y41-N501*Y	x	x
Y41-T500	x	x
Q42-G466	x	x
Q42-Y489	x	x
Y83-N487	\checkmark	\checkmark
K353-G502	x	\checkmark
R393-Y505*H	x	x
D30-K417*N	x	x

form strong hydrophobic interactions in case of akummicine N-oxide. Apart from the type of interactions between the ligand and the protein, the binding energetics was observed by calculating the free energy of binding ($\Delta\Delta G_{\text{bind}}$) between the two. Fig. 13 shows the $\Delta\Delta G_{\text{bind}}$ throughout the simulations for the M^{Pro}-Aku system. It ranged between -35 and -20 kcal/mol. The $\Delta\Delta G_{\text{bind}}$ was observed to improve as the simulation progressed towards 100 ns?

3.5.2. Interactions with RBD Spike-ACE2 complex

The presence of akummicine N-oxide lead to some crucial alterations in terms of the interactions between RBD Spike and ACE2 receptor. K417, G446, Y449, N487, Y489, Q493, T500, N501, G502 and Y505 from the wild type RBD Spike are known to be involved in interacting with the interface residues of ACE2 (PDB ID: 6LZG) (Wang et al., 2020). In order to understand the involvement of these residues in forming interactions between omicron variant of RBD Spike and human ACE2 receptor, the hydrogen bonding and hydrophobic interactions were calculated. Fig. 14 A and B represent hydrogen bonding (green) and hydrophobic (red) interactions that were lost and gained in the presence of akummicine N-oxide, respectively. The interaction between the residue pairs involved in both hydrogen bonding and hydrophobic have been depicted in blue.

Fig. 14 A shows that two hydrogen bonds, fourteen hydrophobic interactions and three RBD Spike-ACE2 interactions involved in both hydrogen bonding and hydrophobic in the SA-Apo system. These interactions were observed to be completely absent in the SA-Aku system. Fig. 14 B shows that a single hydrogen bond, ten hydrophobic interactions and three RBD Spike-ACE2 interactions were involved in both hydrogen bonding and hydrophobic in the SA-Aku system. These interactions were observed to be newly formed in the SA-Aku system. The wild type RBD Spike-ACE2 receptor are known to form thirteen stable hydrogen bonds between each other. These hydrogen bonds have been listed in Table 1.

Table 1 also states whether these hydrogen bonds were observed in the SA-Apo and SA-Aku simulation systems. Q24-N487 and Y83-N487 these two hydrogen bonds were observed to be stable in SA-Apo and SA-Aku simulation systems. Eight hydrogen bonds were formed neither in the SA-Apo or SA-Aku simulation systems. The hydrogen bonding between D38-Y449 was retained in the SA-Apo system, whereas it was completely lost in SA-Aku system. The K353-G502 hydrogen bond formed in the SA-Aku system, however, in case of SA-Apo the K353 of ACE2 interacted with T500. Similarly, E35-R493 (Q493R mutation) hydrogen bond was observed in SA-Aku system, which was compensated by H34-R493 interaction in the SA-Apo system.

The interaction analysis suggested that the omicron variant of RBD Spike formed few new interactions as compared to the wildtype with the ACE2 receptor. The presence of akummicine N-oxide led to loss of few this crucial interactions, thereby reducing the binding between RBD spike and ACE2 receptor. This finding has been further supported by MMGBSA free energy between RBD-Spike and ACE2 (Fig. 14 C). Fig. 14 C depicts the normalized $\Delta\Delta G_{\text{bind}}$ between RBD Spike and ACE2 receptor in the SA-Apo and SA-Aku simulation systems. It was observed that the binding is affected in the presence of akummicine N-oxide. The free energy value increases in the SA-Aku system, which indicates that the binding was weakened in the presence of akummicine N-oxide.

The binding of the akummicine N-oxide with the RBD Spike-ACE2 complex was analysed for the SA-Aku simulation system. Fig. 15 A shows the akummicine N-oxide interacting residues from RBD Spike and ACE2 receptor. H34, P389, R393 and A387 from ACE2 as well as F375, R403, R408, D405, G404, V503, G504 and Y508 from RBD Spike of the omicron variant were observed to form hydrogen bonding and/or hydrophobic interactions with the ligand molecule. F375 is a part of the mutations that occur in the omicron variant of RBD Spike. Fig. 15 B shows the $\Delta\Delta G_{\text{bind}}$ between akummicine N-oxide and RBD Spike-ACE2 complex. The free energy of binding was observed to improve by the end of 100ns of the simulations.

3.6. Drug likeliness properties of the phytochemicals

The drug likeliness properties of the four phytochemicals were obtained from the SwissADME server (Daina et al., 2017) (Table 2). All the four phytochemicals were observed to be soluble and having high gastrointestinal absorption.

4. Concluding remarks

The ensemble docking protocol helps to explore the different conformations the drug binding pocket may attain in the drug target being addressed. Using MD simulations and clustering approach it was observed that the M^{Pro} and RBD-spike of Omicron variant of SARS-CoV-2 sample multiple conformational ensembles. Docking these individual ensemble representatives with akummicine-N-oxide, akummiginone, echitamidine-n-oxide, and echitaminic acid revealed that the binding was better in case of the mutant as compared to the wild type. Molecular

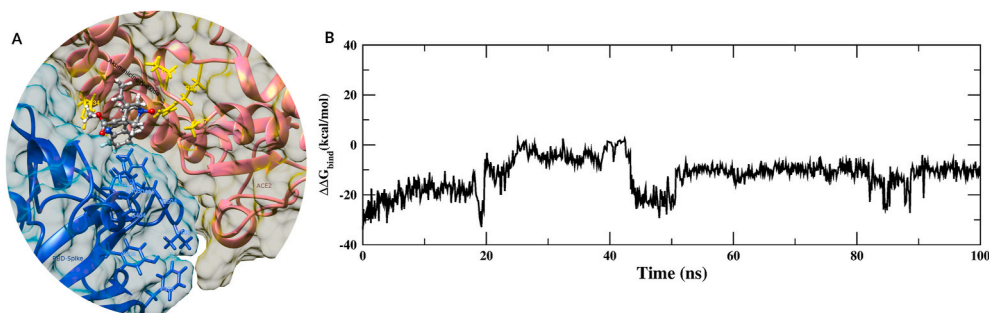


Fig. 15. (A) Residues from RBD Spike-ACE2 complex interacting with akummicine N-oxide. (B) $\Delta\Delta G_{\text{bind}}$ between akummicine N-oxide and RBD Spike-ACE2 complex.

Table 2
Drug likeness properties of the four phytochemicals from AYUSH-64 considered in this study.

Molecule	Molecular weight (kDa)	No. of H-bond acceptors	No. of H-bond donors	Total Surface Area	Lipophilicity (WLOGP)	Solubility	GI absorption	BBB permeability	Pgp substrate	CYP3A4 Inhibitor	log Kp (cm/s)	Lipinski #violations
Akummicine-N-oxide	338.4	3	1	67.76	1.89	Soluble	High	Yes	Yes	No	-7.02	2
Akumiginone	367.42	4	2	75.63	0.57	Soluble	High	No	Yes	No	-8.01	2
Echitamidine-n-oxide	356.42	4	2	87.99	1.44	Soluble	High	Yes	Yes	Yes	-7.45	0
Echitaminc acid	371.45	4	4	89.79	0.42	Soluble	High	Yes	Yes	Yes	-8.27	0

dynamics simulations of akummicine N-oxide bound M^{PRO} and omicron variant of RBD Spike-ACE2 receptor complex showed significant changes in the conformational changes. PCA showed the specific regions that were observed to deviate from the wild type conformation in the presence of the ligand. The residues of M^{PRO} interacting with the akummicine N-oxide were observed to be the ones crucial for forming stable interactions with ligands. In case of RBD Spike-ACE2 complex, the interaction between the two proteins was observed to weaken to a small extent in the presence of akummicine N-oxide. The MM-GBSA binding energetics was observed to support this finding. Hence, it can be inferred that, these phytochemicals from AYUSH-64 formulation may have the potential to act against the Omicron variant of SARS-CoV-2.

CRediT authorship contribution statement

Vinod Jani: Conceptualization, Methodology, Validation, Formal analysis, Writing – original draft, Funding acquisition, Project administration. **Shruti Koulgi:** Conceptualization, Methodology, Validation, Formal analysis, Writing – original draft, Funding acquisition, Project administration. **Mallikarjunachari V.N. Uppuladinne:** Conceptualization, Methodology, Validation, Formal analysis, Writing – original draft, Funding acquisition, Project administration. **Saket Ram Thrigulla:** Resources, Writing – review & editing, Supervision, Project administration, Funding acquisition. **Manohar Gundeti:** Resources, Writing – review & editing, Supervision, Project administration. **Goli Penchala Prasad:** Resources, Writing – review & editing, Supervision, Project administration. **Sanjaya Kumar:** Resources, Writing – review & editing, Supervision, Project administration. **Srikanth Narayanam:** Resources, Writing – review & editing, Supervision, Project administration. **Uddhavesh Sonavane:** Resources, Writing – review & editing, Supervision, Project administration, Funding acquisition. **Rajendra Joshi:** Resources, Writing – review & editing, Supervision, Project administration, Funding acquisition.

Declaration of competing interest

The authors declare that they have no known competing financial interests or personal relationships that could have appeared to influence the work reported in this paper.

Data availability

Data will be made available on request.

Acknowledgements

The authors would like to acknowledge the Bioinformatics Resources and Applications Facility (BRAf) for providing the computing infrastructure and support. The work was funded by the Ministry of Electronics and Information Technology and Department of Science and Technology, Government of India under the National Supercomputing Mission. The work was also funded by the Central Council for Research in Ayurvedic Sciences under intra-mural projects.

Appendix A. Supplementary data

Supplementary data to this article can be found online at <https://doi.org/10.1016/j.crstbi.2024.100151>.

References

- Allen, W.J., Balias, T.E., Mukherjee, S., Brozell, S.R., Moustakas, D.T., Lang, P.T., Case, D.A., Kuntz, I.D., Rizzo, R.C., 2015. Dock 6: impact of new features and current docking performance. *J. Comput. Chem.* 36 (15), 1132–1156. <https://doi.org/10.1002/JCC.23905>.
- Allerton, C.M.N., Arcari, J.T., Aschenbrenner, L.M., Avery, M., Bechle, B.M., Behzadi, M. A., Boras, B., Buzon, L.M., Cardin, R.D., Catlin, N.R., Carlo, A.A., Coffman, K.J.,

- Dantonio, A., Di, L., Eng, H., Farley, K.A., Ferre, R.A., Gernhardt, S.S., Gibson, S.A., Greasley, S.E., Greenfield, S.R., Hurst, B.L., Kalgutkar, A.S., Kimoto, E., Lanyon, L.F., Lovett, G.H., Lian, Y., Liu, W., Martínez Alsina, L.A., Noell, S., Obach, R.S., Owen, D. R., Patel, N.C., Rai, D.K., Reese, M.R., Rothan, H.A., Sakata, S., Sammons, M.F., Sathish, J.G., Sharma, R., Stepan, C.M., Tuttle, J.B., Verhoest, P.R., Wei, L., Yang, Q., Yurgeloni, L., Zhu, Y., 2024. A second-generation oral SARS-CoV-2 main protease inhibitor clinical candidate for the treatment of COVID-19. *J. Med. Chem.* 30 <https://doi.org/10.1021/acs.jmedchem.3c02469>. Epub ahead of print. PMID: 38687966.
- AMBER 2020, 2020.
- Cha-Silva, A.S., Gavaghan, M.B., Bergroth, T., Alexander-Parrish, R., Yang, J., Draica, F., Patel, J., Garner, D.A., Stanford, R.H., Meier, G., McLaughlin, J.M., Nguyen, J.L., 2024. Effectiveness of nirmatrelvir-ritonavir for the prevention of COVID-19-related hospitalization and mortality: a systematic literature review. *Am. J. Therapeut.* 31 (3), e246–e257. <https://doi.org/10.1097/MJT.0000000000001744>. Epub 2024 Apr 29. PMID: 38691664; PMCID: PMC11060058.
- Chopra, A., Tillu, G., Chuadhary, K., Reddy, G., Srivastava, A., Lakdawala, M., Gode, D., Reddy, H., Tamboli, S., Saluja, M., Sarmukaddam, S., Gundeti, M., Raut, A.K., Rao, B. C.S., Yadav, B., Srikanth, N., Patwardhan, B., 2023. Co-administration of AYUSH 64 as an adjunct to standard of care in mild and moderate COVID-19: a randomized, controlled, multicentric clinical trial. *PLoS One* 18 (3), e0282688. <https://doi.org/10.1371/JOURNAL.PONE.0282688>.
- Daina, A., Michielin, O., Zoete, V., 2017. SwissADME: a free web tool to evaluate pharmacokinetics, drug-likeness and medicinal chemistry friendliness of small molecules. *Sci. Rep.* 7 <https://doi.org/10.1038/SREP42717>.
- Davidchack, R.L., Handel, R., Tretyakov, M.V., 2009. Langevin thermostat for rigid body dynamics. *J. Chem. Phys.* 130 (23) <https://doi.org/10.1063/1.3149788>.
- Ester, M., Kriegl, H., Sander, J., Xu, X., 1996. A density-based algorithm for discovering clusters in large spatial databases with noise. In: *Proceedings of the Second International Conference on Knowledge Discovery and Data Mining*, KDD-96), pp. 226–231.
- GetContacts.
- Gundeti, M.S., Bhurke, L.W., Mundada, P.S., Murudkar, S., Surve, A., Sharma, R., Mata, S., Rana, R., Singhal, R., Vyas, N., Khanduri, S., Sharma, B.S., Srikanth, N., Dhiman, K.S., 2022. AYUSH 64, a polyherbal ayurvedic formulation in influenza-like illness - results of a pilot study. *J. Ayurveda Integr. Med.* 13 (1) <https://doi.org/10.1016/j.jaim.2020.05.010>.
- H Ali, A., Altheety, M., Hasen Alubaidy, M., Dohare, S., 2022. Nano drug (AgNPs capped with hydroxychloroquine): synthesis, characterization, anti-covid-19 and healing the wound infected with *S. aureus*. *Mater. Chem. Phys.* 287, 126249 <https://doi.org/10.1016/j.matchemphys.2022.126249>. Epub 2022 May 12. PMID: 35581994; PMCID: PMC9096690.
- Humphrey, W., Dalke, A., Schulten, K., 1996. VMD: visual molecular dynamics. *J. Mol. Graph.* 14 (1), 33–38. [https://doi.org/10.1016/0263-7855\(96\)00018-5](https://doi.org/10.1016/0263-7855(96)00018-5).
- Jani, V., Koulgi, S., Uppuladinne, V.N.M., Sonavane, U., Joshi, R., 2021. An insight into the inhibitory mechanism of phytochemicals and FDA-approved drugs on the ACE2-spike complex of SARS-CoV-2 using computational methods. *Chem. Zvesti* 75 (9), 4625–4648. <https://doi.org/10.1007/s11696-021-01680-1>.
- Jin, Z., Du, X., Xu, Y., Deng, Y., Liu, M., Zhao, Y., Zhang, B., Li, X., Zhang, L., Peng, C., Duan, Y., Yu, J., Wang, L., Yang, K., Liu, F., Jiang, R., Yang, X., You, T., Liu, X., Yang, X., Bai, F., Liu, H., Liu, X., Guddat, L.W., Xu, W., Xiao, G., Qin, C., Shi, Z., Jiang, H., Rao, Z., Yang, H., 2020. Structure of Mpro from SARS-CoV-2 and discovery of its inhibitors. *Nature* 582 (7811), 289–293. <https://doi.org/10.1038/S41586-020-2223-Y>.
- Koulgi, S., Jani, V., Uppuladinne, M., Sonavane, U., Nath, A.K., Darbari, H., Joshi, R., 2021. Drug repurposing studies targeting SARS-CoV-2: an ensemble docking approach on drug target 3C-like protease (3CLpro). *J. Biomol. Struct. Dyn.* 39 (15), 1–21. <https://doi.org/10.1080/07391102.2020.1792344>.
- Maier, J.A., Martinez, C., Kasavajhala, K., Wickstrom, L., Hauser, K.E., Simmerling, C., 2015. Ff14SB: improving the accuracy of protein side chain and backbone parameters from Ff99SB. *J. Chem. Theor. Comput.* 11 (8), 3696–3713. <https://doi.org/10.1021/ACS.JCTC.5B00255>.
- Medhi, R., Srinoi, P., Ngo, N., Tran, H.V., Lee, T.R., 2020. Nanoparticle-based strategies to combat COVID-19. *ACS Appl. Nano Mater.* 3 (9), 8557–8580. <https://doi.org/10.1021/acsnano.0c01978>. PMID: 37556239.
- Miller, B.R., McGee, T.D., Swails, J.M., Homeyer, N., Gohlke, H., Roitberg, A.E., 2012. MMPBSA.py: an efficient program for end-state free energy calculations. *J. Chem. Theor. Comput.* 8 (9), 3314–3321. <https://doi.org/10.1021/CT300418H>.
- Ram, T.S., Munikumar, M., Raju, V.N., Devaraj, P., Boiroju, N.K., Hemalatha, R., Prasad, P.V.V., Gundeti, M., Sisodia, B.S., Pawar, S., Prasad, G.P., Chincholikar, M., Goel, S., Mangal, A., Gaidhani, S., Srikanth, N., Dhiman, K.S., 2022. In silico evaluation of the compounds of the ayurvedic drug, AYUSH-64, for the action against the SARS-CoV-2 main protease. *J. Ayurveda Integr. Med.* 13 (1) <https://doi.org/10.1016/J.JAIM.2021.02.004>.
- Spoel, D.V.D., Lindahl, E., Hess, B., Groenhof, G., Mark, A.E., Berendsen, H.J.C., 2005. GROMACS: fast, flexible, and free. *J. Comput. Chem.* 26 (16), 1701–1718. <https://doi.org/10.1002/JCC.20291>.
- Srikanth, N., Kumar, A., Chandrasekhararao, B., Singhal, R., Yadav, B., Khanduri, S., Jameela, S., Rai, A.K., Tripathi, A., Rana, R., Ahmad, A., Sharma, B.S., Jaiswal, A., Kotecha, R., 2022. Disease characteristics, care-seeking behavior, and outcomes associated with the use of AYUSH-64 in COVID-19 patients in home isolation in India: a community-based cross-sectional analysis. *Front. Public Health* 10.
- Tang, Z., Kong, N., Zhang, X., Liu, Y., Hu, P., Mou, S., Liljeström, P., Shi, J., Tan, W., Kim, J.S., Cao, Y., Langer, R., Leong, K.W., Farokhzad, O.C., Tao, W., 2020. A materials-science perspective on tackling COVID-19. *Nat. Rev. Mater.* 5 (11), 847–860. <https://doi.org/10.1038/s41578-020-00247-y>. Epub 2020 Oct 14. PMID: 33078077; PMCID: PMC7556605.
- Thakar, A., Panara, K., Goyal, M., Kumari, R., Sungchol, K., 2023. AYUSH (Indian system of medicines) therapeutics for COVID-19: a living systematic review and meta-analysis (first update). *J. Integr. Complement. Med.* 29 (3), 139–155. <https://doi.org/10.1089/JICM.2022.0559>.
- Wang, Q., Zhang, Y., Wu, L., Niu, S., Song, C., Zhang, Z., Lu, G., Qiao, C., Hu, Y., Yuen, K. Y., Wang, Q., Zhou, H., Yan, J., Qi, J., 2020. Structural and functional basis of SARS-CoV-2 entry by using human ACE2. *Cell* 181 (4), 894–904. <https://doi.org/10.1016/J.CELL.2020.03.045>.
- Yamamoto, Y., Inoue, T., 2024. Current status and perspectives of therapeutic antibodies targeting the spike protein S2 subunit against SARS-CoV-2. *Biol. Pharm. Bull.* 47 (5), 917–923. <https://doi.org/10.1248/bpb.b23-00639>. PMID: 38692869.